Virtual Laser Cutting Simulation for Real Parameter Optimization

Dirk PETRING

Fraunhofer Institute for Laser Technology ILT, Steinbachstrasse 15, 52074 Aachen, Germany

Theoretical laser cutting models provide solutions which vary from analytical steady-state equations, generally describing singular physical sub-processes, to fully numerical time dependent simulations requiring several days for the calculation of a single cut. In order to solve this dilemma CALCut calculates the steady-state process including all relevant sub-processes by a combination of semi-analytical and semi-numerical algorithms. Systematic parameter screening is enabled and parameters for high cutting efficiency and quality are identifiable.

Keywords: laser beam cutting, model, simulation, parameters, process optimization

1. Introduction

Only a calculable process can be entirely mastered. In view of the dynamical development of manufacturing technologies in a global market this capability is increasingly recognized as precondition for sustainable success – also in the laser cutting business. If speculations are replaced by trustworthy calculations, a new quality of process understanding can be created.

Against this background the debate about the performance of CO_2 laser and fiber laser cutting systems goes on. Beside experimental work, process diagnostics and theoretical considerations gain attention. The latter vary from simple analytical equations generally describing singular physical sub-processes (see excellent examples in [1]) to fully numerical simulation tools requiring at least several days for the calculation of a short cutting track for one single parameter (see excellent examples in [2]).

Many fundamental questions remain. Some of them are now answered with the help of the simulation tool CALCut, such as: Which melt film surface temperatures do occur? How do multiple reflections (MR) contribute to the process? What are the essential mechanisms of kerf formation? Why do “black knots” and trisections arise in striation patterns?

Hitherto, the experts did not come at all to a consolidated understanding of these issues and to an explanation of their parameter dependencies even less - mainly because most parameter dependencies show highly nonlinear behaviour. [3]

Systematic calculations based on the comprehensive steady-state cutting model and simulation tool CALCut [4, 5] shall support parameter screening and reveal new insights. The calculation of the steady-state process by a combination of semi-analytical and semi-numerical algorithms is demonstrated to be an effective way to **improve process understanding.** Based on well-defined criteria process regimes for optimized cutting efficiency and cut quality become identifiable. The simulation-supported parameter screening is believed to take on a key role in future development of laser materials processing**.**

2. Model and simulation of the cutting front

The unprecedented scope of the physical sub-processes included in CALCut enables the three-dimensional stationary cutting front geometry and the resulting cut kerf geometry to be calculated.

CALCut takes into account the material, material thickness, laser wavelength, beam quality, beam power and power density distribution, polarization, raw beam diameter, focusing optics, focal length, focal position, cutting gas type and pressure as well as the cutting speed.

CALCut identifies the spatial distributions of the absorbed laser beam power density, of the temperature, of thickness and flow velocity of the melt film along with the evaporation rates and pressure gradients. Automatic iteration determines the maximum cutting speed. The analysis of the cutting front geometry and the above mentioned distribution functions also allows conclusions to be drawn about the achievable cut quality.

2.1 The model

In a closed formulation, the three-dimensional, steady-state model links the sub-processes of beam focusing, beam propagation, Fresnel absorption and reflection, compressible cutting gas flow, exothermic reaction (when indicated), heat conduction, phase transformation into the molten and vaporous states and mass transport due to melt and vapor flows taking into account the shear-stress induced by the cutting gas flow, capillary forces due to surface tension and driving forces due to vapor pressure gradients [4, 5]. The viscous melt is treated as a Newtonian fluid.

The cutting gas flow is modelled as a function of the cutting gas type and the cutting gas pressure and depends on the geometry and temperature of cutting front and kerf. Below the nozzle exit, the gas jet is assumed to initially expand isentropicly and subsequently, via a normal compression shock above the workpiece, experiences an increase in entropy. This is taken into account as a loss in static pressure before the second isentropic expansion in the kerf. The resulting flow rate in the kerf is calculated.

The locally induced shear stress is estimated according to the laws of turbulent channel flow. The maximum penetration depth of the supersonic flow field – here called "maximum jet penetration" - is determined by calculating the flow distance where the highest physically allowable pressure increase due to the friction losses occurs. This part of the model makes use of the conservation equations for compressible tubular flow in isothermal approximation [4].

In the steady-state equilibrium, the cutting front arises in such a way that the locally absorbed power density corresponds to the local heat-flow requirement. Beside the power balance, mass and force balance have to be fulfilled simultaneously.

The parameterization of the cutting front is based on vertically stacked, semicircular cutting front segments of defined height being horizontally resolved by discrete facets. The shape and position of every single segment is parameterized by its height, curvature radius, melt film thickness, vertex and flank inclinations and its horizontal distance from the laser beam axis in cutting direction.

The above mentioned power, mass and force balances and a boundary layer approximation of the heat flow at the flank as well as two continuity conditions for vertex and flank provide the governing equations to be solved for the calculation of each segment (**fig. 1**).

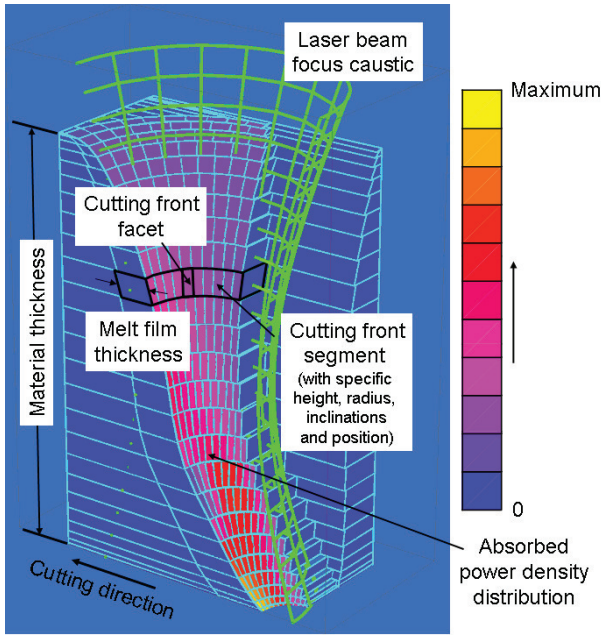

Fig. 1 CALCut simulation of a laser cutting front.

2.2 The simulation tool CALCut

A simplified flow-chart of the corresponding simulation program is sketched in **fig. 2** [4, 5].

The computer simulation CALCut has now been used for more than twenty years to predict, analyze and optimize the performance of various cutting applications (see [6] and references therein). The wide range of validity of CALCut has been demonstrated by verifying the calculations with experimental variations of material, sheet thickness, laser beam power, cutting speed, focal length, focal position and polarization.

As part of this work, three cutting process regimes have been identified: the heat-conduction-controlled process at low speeds, the melting-controlled process in the medium speed range and the evaporation-controlled process above a critical cutting speed [4].

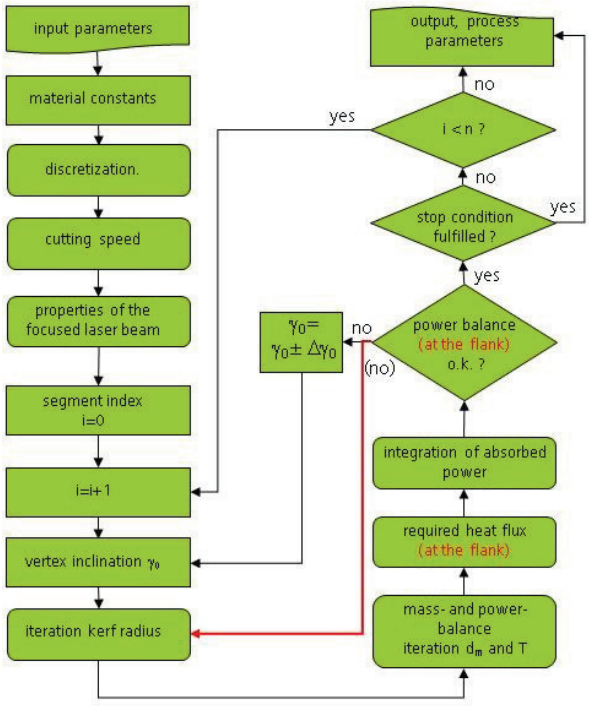

Fig. 2 Simplified flow-chart of CALCut.

With the aim of reaching cutting processes that are as efficient as possible and that provide high-quality cutting results, the following simulation indicators are provided by CALCut and represent most crucial features to be assessed:

- maximum cutting speed,
- maximum jet penetration,
- irregularity of the cutting front geometry,
- cutting front robustness with incremental changes of parameters (not discussed in this paper).

As a result, efficient and robust regimes can be identified along with an appropriate cutting speed and suitable optical parameters. In fact, such simulation-supported parameter screening has already been used to achieve an adequate design of a cutting head with zoom optics [7].

3. Simulation results

3.1 Fundamental issues

Thick sections benefit from the larger Brewster angle at the 10.6µ wavelength of CO_2 lasers, leading to an increased absorptance in metals at grazing incidence. This situation is a stroke of luck for CO_2 lasers and it modifies some oversimplified statements frequently made, inadmissibly generalizing the high absorption at 1µ wavelength at perpendicular incidence, i.e. at small angles of incidence. Looking furthermore at the projected absorptance, it becomes obvious that its progressive increase with decreasing angle suggests a significant sensitivity to perturbations at 1µ (see **fig. 3**) [6].

This understanding of the Fresnel effect is helpful but the real process is more complicated. For a comprehensive and detailed process analysis an appropriate simulation is essential.

One question is: Are there further peculiarities of beam coupling during cutting steel with 1µ wavelength compared to 10µ wavelength?

While the relevance of the Brewster angle is evident, some authors nevertheless assume better wave-guiding through multiple reflections in case of 10.6µ compared to 1µ [8]. It is demonstrated in [6] that the physics of Fresnel absorption bring about something else.

Fig. 4 presents two curves of maximum cutting speed versus power calculated with CALCut for the same application. In the bottom curve only the first absorption step without subsequent multiple reflections and in the top curve all multiple reflections and absorption steps on the self-adjusting cutting front are taken into account.

In accordance with the assumptions in [9, 10] and in contrast to the assumption in [11], an improved beam coupling further down the cutting front due to multiple reflections occurs. A correct simulation taking MR into account provides realistic results regarding cutting depth and maximum achievable cutting speed. The absorption at 1µ would be much lower (especially but not only in thick sections) if this "wave-guiding" would not occur. In the example in **fig. 4** the coupling efficiencies without and with MR differ by a factor of two [6].

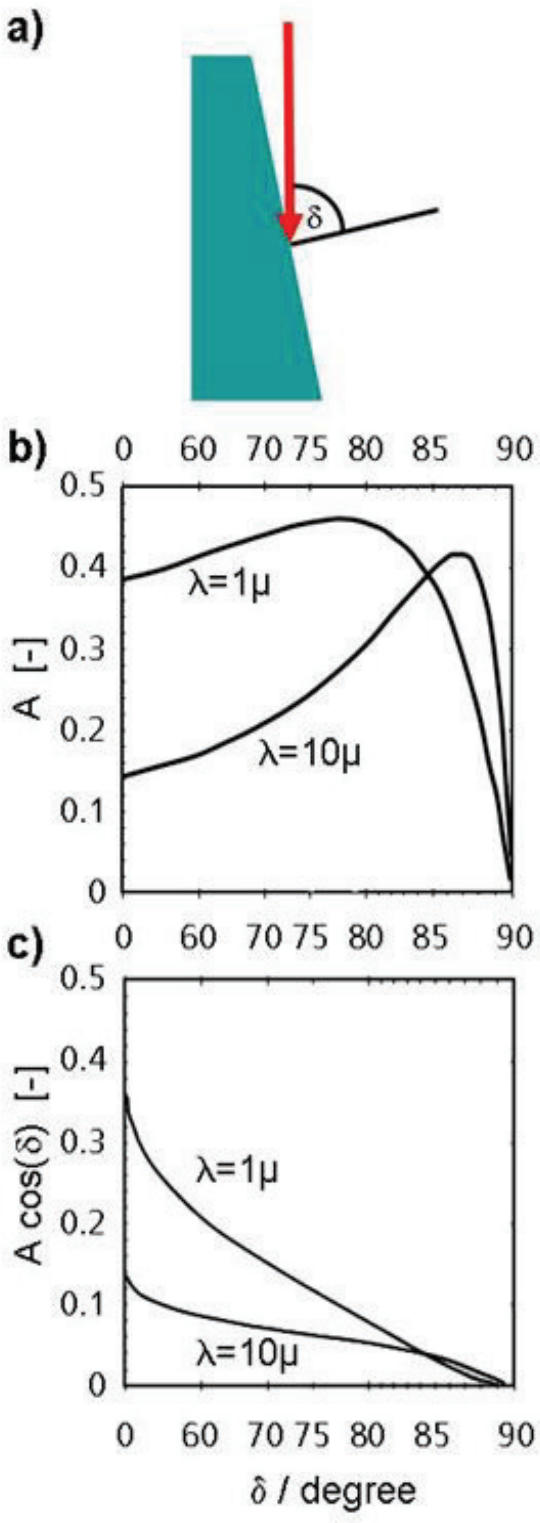

Fig. 3 Fresnel absorption of circularly or randomly polarized light for steel at a melt surface temperature of 2500 K, calculated according to [4]; a) definition of the angle of incidence δ; b) absorptance (A) as a function of angle of incidence; c) projected absorptance.

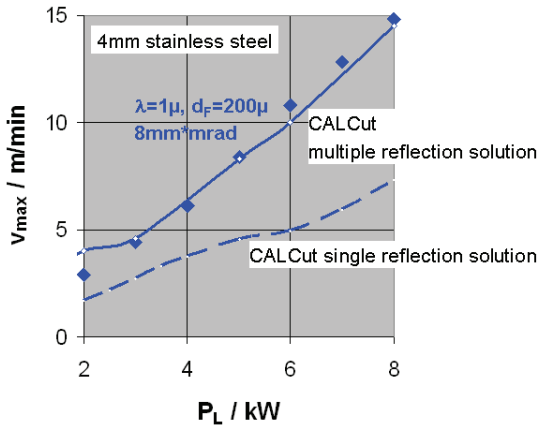

Fig. 4 Only by taking into account multiple reflections 1 micron cutting speeds become explainable.

The effects of MR contributions at 1µ can be made plausible with the simplified illustration in **fig. 5** [3]. In narrow convergent channels like in a cutting kerf along a cutting front the first point of incidence of a ray is characterized by a relatively large angle of incidence and thus leads to low or medium absorption in case of 1µ radiation. At the finite radius of the kerf entrance (not sketched in **fig. 5**), where the transition from sheet surface to kerf entrance takes place, smaller angles of incidence can result in high absorptance of the outer low intensity parts of the beam boundary. However, the main parts of the beam are acting below this upper edge with large angles of incidence. During numerous MR steps the angle of incidence gets continuously smaller, leading to continuously increased absorptance down the kerf channel or cutting front, respectively.

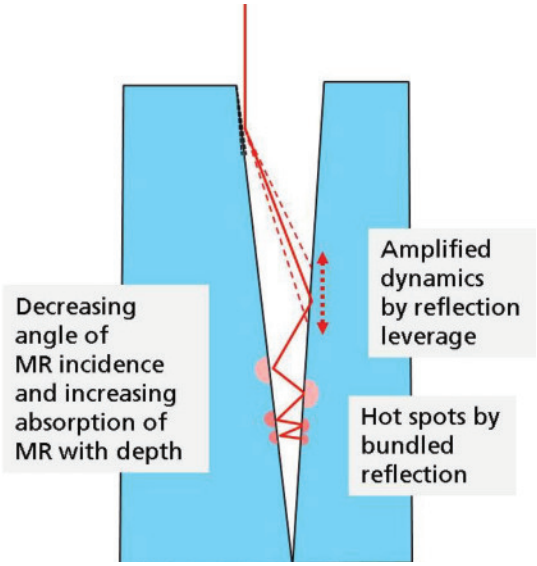

Fig. 5 Effects of multiple-reflections are getting more pronounced at 1 micron wavelength due to low absorption at grazing incidence and increasing absorption with decreasing angle of incidence (strongly simplified sketch for illustration only).

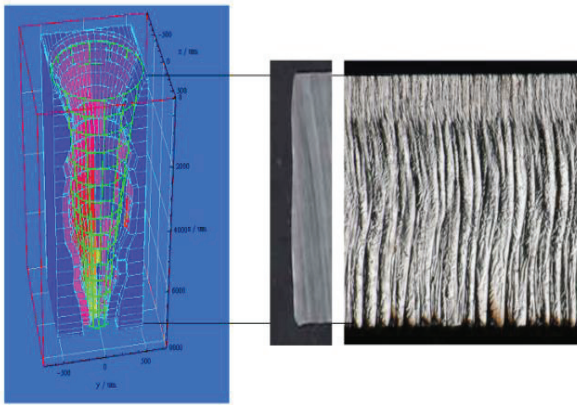

Fig. 6 Theoretical and practical evidence of multiple reflections by undercut formation (laser TruDisk 8002 @ 8 kW, combi-head Laserfact F2-Y, 8 mm structural steel, cutting speed 2.4 m/min, cutting gas: nitrogen).

Moreover, hot spots due to self-focusing effects in the kerf can be produced (**fig. 5**). They are also identified in CALCut simulations. **Fig. 6** presents a cutting front geometry calculated with CALCut for thicker section cutting, taking into account all multiple reflections and absorption steps on the self-adjusting cutting front – partly visible as hot spots of the energy flux distribution I_{abs} on the right half representation of the simulated front. Accordingly, an irregular and locally widened kerf geometry occurs. This undercut is also visible at the real cut edge in **fig. 6** [6]. The hot spots can even reach the kerf walls behind the cutting front and cause irregular front and kerf shapes and induce melt flow irregularities with related quality losses.

The simulated cutting fronts in **fig. 7** ultimately depict the different characteristics depending on the wavelength [3]. It has to be pointed out that beside the wavelengths, differing by a factor of 10, and the power, taken a little bit higher in case of the CO_2 laser, all other parameters have been selected identical, including the focal geometry (diameter and Rayleigh-length). The values are given in **fig. 7** and its caption. At least a quite similar change of the temperature level with speed occurs for both wavelengths, reaching vaporization temperature at about 5 m/min. The variation of speed has much higher influence on temperature than the wavelengths under consideration. Nevertheless, a slightly higher temperature is calculated at 1 micron compared to 10 micron, in contrast to the assumption in [12] where a lower temperature is predicted.

As already emphasized, at the kerf entrance radius the higher absorption of 1 micron radiation at small angles of incidence becomes effective. Even the low intensity regime of the beam boundary, normally in the case of 10 micron being wasted by reflection from the sheet surface, can melt the material and leads to a wider kerf entrance in case of the 1 micron wavelength. This can be clearly read from the simulated cutting fronts in **fig. 7**. It is also evident that the effective MR widens the kerf cross-section during the further propagation of the light down the kerf.

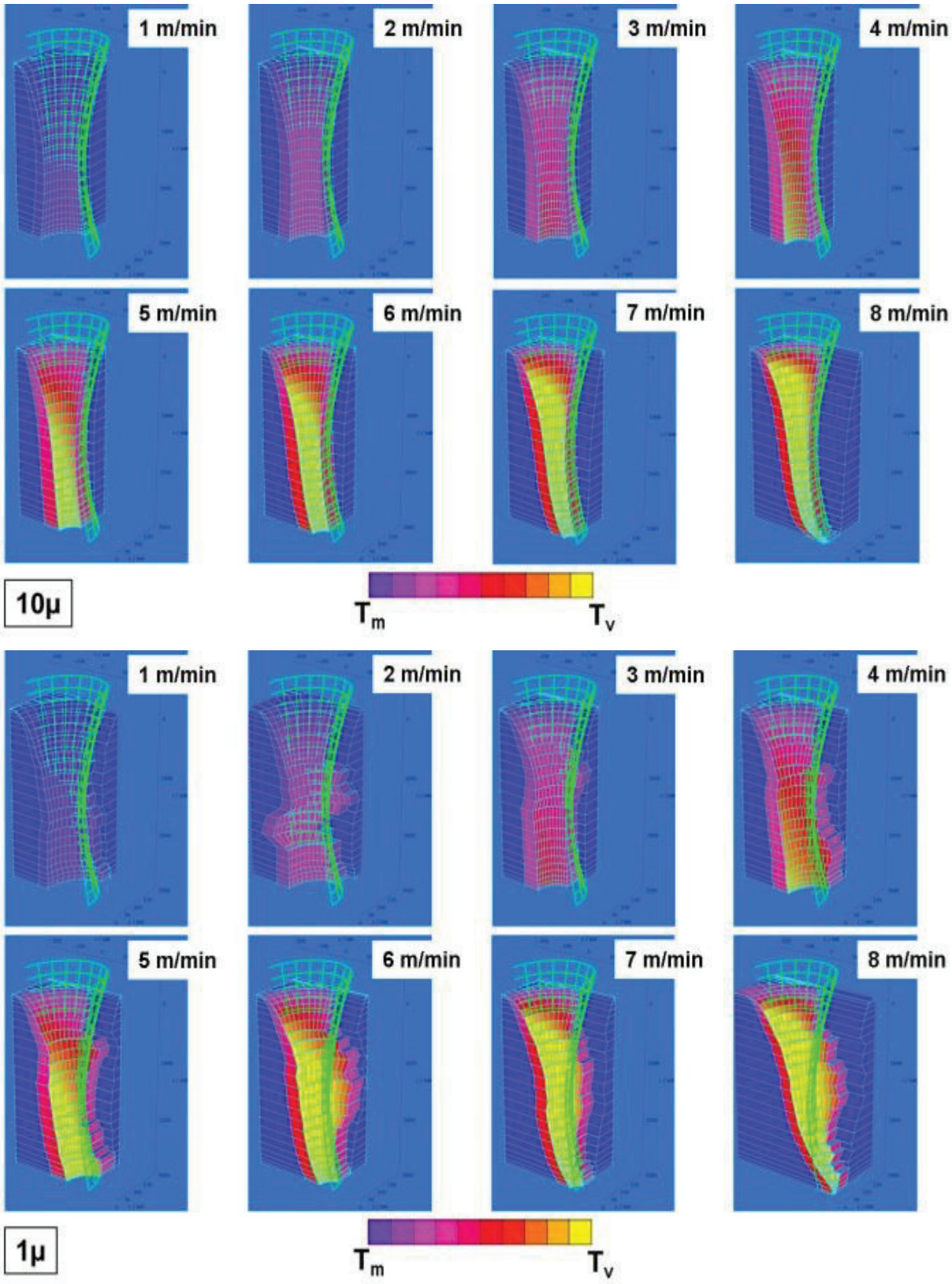

Fig. 7 CALCut simulations of cutting fronts in 3 mm stainless steel. Focus diameter 150 µm, Rayleigh-length 1.25 mm, laser beam power 3 kW @ 1µm and 3.5 kW @ 10µm, focal position -1.5 mm (below surface), cutting gas nitrogen @ 1.7 MPa. More expanded and irregular cutting fronts in case of 1 micron (bottom) compared to 10 micron (top) wavelength.

Even more obvious are the buckled cutting front geometries partly extended in the cutting direction in case of 1 micron. This has also been observed experimentally in an excellent investigation of [10] and is a clear consequence of the MR. In comparison, in case of 10 micron the shapes of the cutting fronts are smooth and regular.

Careful evaluation of simulations such as those in **figs. 6-7** reveal that MR contributions typically start at 1-2 mm cutting depth. This is in good agreement with the related experimental findings of the transition between fine and rougher cut edge regions and in contrast to the assumptions in [13]. In this context it is important to note that multiple reflections can destabilize the lower cutting zone and lead to coarser striations [6]. This is also illustrated in **fig. 5**, where amplification of dynamics by the reflection leverage is sketched.

3.2 Finding quality indicators by simulation

Parameters

Further detailed practical and theoretical investigations have been carried out on cutting 8 mm stainless steel with a fiber laser at 3.75 kW beam power using a 100 µm diameter fiber. The focus diameter was 250 µm and the Rayleigh-length was 4.8 mm. Cutting gas was nitrogen being used at a pressure of 2 MPa. All cuts have been performed and calculated at a cutting speed of 1.8 m/min.

Evaluation procedure

Main concern was with the influence of the focal position on the properties of the cut flanks. Therefore, the focal position was varied in a wide range (see **figs. 8-13**). **Figs. 8-10** and **fig. 12** show representations of the calculated kerf cross-section and front vertex (stretched by a factor of 3.6) as well as photos of related practically produced cut flanks and cross-section – partially also stretched by a factor of 3.6 for easier assessment. Moreover, the maximum values of the averaged roughness R_z of the cut flanks (**fig. 11**) and the maximum dross length (**fig. 13**) are correlated with "indicator" values provided by CALCut.

Indication of irregularities on the cut flank

One fundamental question during cutting process development with 1 micron lasers is: Why do "black knots" and trisections arise on the striation pattern of the cut flanks? These kinds of irregularities are definitely unwanted in practical applications of industrial laser cutting. They are first of all a more qualitative than quantitative issue. For industrial customers regularity of the striation pattern is more important than the mere roughness value of the cut flank. The understanding of irregularities' origin helps to find parameter regimes and advanced optical designs which avoid their occurrence.

It has been found out that beam parameters are much more relevant for these phenomena than gas parameters. Inappropriate cutting gas parameters and nozzle design can superimpose or hide these effects by additional mechanisms related to the melt flow in the cut kerf. Nevertheless, the basic origin is the formation of the cutting front geometry according to the power density and poynting-vector distribution and the interaction and further propagation of the laser beam.

The comparison of simulated and practical cut results in **fig. 8** and **fig 9** demonstrate exemplarily the strong correlation of the profile of the calculated steady-state cutting front vertex and cutting kerf cross-section with the resulting striation pattern on the practical cut flank. At the selected cutting speed and beam parameters, approximately the first millimeter of the cutting depth evolves solely due to direct illumination and absorption of the laser beam border rays. This region forms the first section of the striation pattern with fine and regular ripples and a smooth top section of the calculated profiles. Propagating in depth, multiple reflections have to support the cutting front and kerf formation in order to fulfill the local power balance of the cut. Depending on the selected focal position pronounced buckles can occur on the cutting front. They generate their finger prints on the resulting cut flank. This causes a further sectioning of the bottom striation pattern up to the formation of what we call "black knots" (see **fig. 8**). Just as irregularities on the calculated profiles generally correlate with corresponding irregularities on the real cut flanks, so more regular, calculated profiles indicate a more regular striation pattern with straight ripples (**fig. 9**).

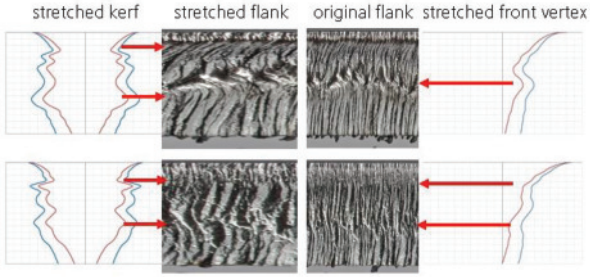

Fig. 8 Indication of irregularities on the cut flank. Trisection of the striation pattern (top and bottom) and "black knots" (top) are indicated by the correspondingly buckled profile of CALCut's simulated kerf cross-section and vertex.
Focal position: top -8mm, bottom -10mm.

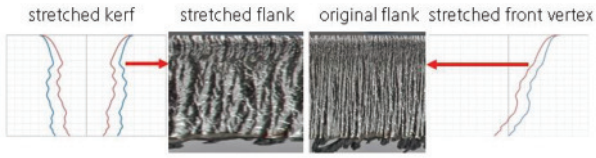

Fig. 9 Smoother profiles of the calculated vertex and flank indicate straighter and more regular striations.
Focal position +6mm.

After this finding it does not surprise that also the characteristic kerf cross-section of a cut is predictable quite reliably by CALCut. However, when looking at a practical cross-sections it has to be born in mind that it only represents a localized part of the whole kerf track in a singular transversal plane. If the cut features coarse, inclined or curved striations the profile of the cross-section very much depends on its location. Therefore, a single cross-section does not definitely represent the whole cut and might even lead to wrong interpretation. Nevertheless, comprehensive and careful investigations revealed that the geometry of the kerf entrance and the qualitative course of the kerf is very well described by the simulation and therefore believed to be predictable by CALCut. The example in **fig. 10** underlines CALCut's capabilities to describe very specific features of kerf formation in laser beam cutting. The kerf entrance geometry, the following kerf expansion as well as the subsequent kerf constriction have theoretically and practically the same appearance.

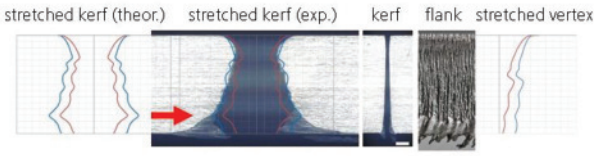

Fig. 10 CALCut's indication of an expanding kerf followed by kerf constriction is in qualitative and quantitative agreement with the practical result. Focal position -2mm.

The red lines indicate the calculated melt surface profile of the cutting front vertex and the cutting flank, respectively – both being characteristic features of the simulated 3-dimensional cutting front. The simulated cutting flank is assumed to form the final cut flank. This assumption seems to be confirmed. The blue lines indicate the melt-solid phase boundary during cutting. In the bottom part of the kerf cross-section the practical extension of the recast is significantly wider than the calculated melt film thickness. The reason is evident. Superheated melt is transported behind the laser-heated cutting front out of the calculation regime of the model. Beside the inertia of the melt being moved together with the workpiece against the cutting direction, additional azimuthal melt acceleration due to vapor pressure gradients on the superheated melt can occur in the deeper kerf sections. The convective heat transport can even results in a post melting of the flank behind the laser-material interaction zone. This is outside of the represented calculation regime but in accordance with the model.

Indication of cut flank roughness

It is far from being evident that a steady-state model and simulation like CALCut can correctly describe various features of a highly dynamic laser beam cutting process. Nevertheless, CALCut seems to be capable of describing parameter dependencies quite accurately not only regarding achievable cutting speed and depth but also regarding quality features. Even if quality features are often thought to be an intrinsic consequence of the dynamics of the process it comes out that first of all the quasi-steady behavior of the process is most crucial and has to be understood and mastered. The reason is obvious. Significantly unsteady process behavior is induced by irregularities of the process interaction zone. In other words, a regular interaction zone is a fundamental requirement for an at least quasi-stable process. Laser beam cutting in most cases of its industrial sheet metal application relies on continuous-wave laser radiation for highest productivity, using beam modulation only at certain circumstances such as piercing and slow cutting in small contours. Also from that point of view it becomes rather logical to deal with the investigation, understanding and optimization of the steady-state. It is worth mentioning that even the sensitivity to perturbations can be predicted by the steady-state approach.

The fine art of laser beam cutting process simulation is the prediction of the cut flank roughness. Being motivated by the above results and considerations regarding a steady-state process with a steady-state (continuous-wave) tool, it becomes evident to check the potential of correlating the calculated irregularities of the simulated cutting front with the practically occurring cut flank roughness. The remaining task is to find an appropriate indicator of the cutting front irregularity. Mathematically, the irregularity of a surface along the path F(z) is given by the total curvature:

$$CF_{irr} = \int_{z1}^{z2} \left[\frac{F''(z)}{(1+F'^2)^{3/2}}\right]^2 dz \qquad (1)$$

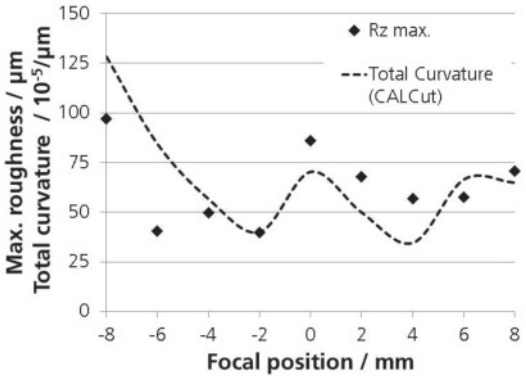

Fig. 11 Correlation of the maximum averaged roughness R_z and CALCut's irregularity indicator "total curvature" versus focal position.

CF_{irr} is calculated by integration along the simulated profiles of the cutting front vertex and the cutting flank from top to bottom of the cutting depth coordinate z in order to provide an indicator for the cut flank roughness. The resulting function (dotted line in **fig. 11**) is compared with the measured maximum values of the averaged roughness of the practically produced cut flanks (rhombi in **fig. 11**).

There are good reasons to exercise some caution regarding the interpretation of **fig. 11**. First of all, the measured R_z-values are the maximum values of 6 measurements, i.e. 3 on both sides of each 100 mm long cut at the respective focal position – taken at a cutting depth of 2, 4 and 6 mm, respectively. It is well known that roughness values of laser cut flanks strongly scatter and very much depend on the measurement position. Moreover, it has to be kept in mind that the dimension of a total curvature is something like an inverse radius and therefore not a length dimension as it is the case with R_z. Against this background, the apparent correlation in **fig 11** is to be treated as a first positive hint. Nevertheless, further investigations have to be performed to confirm the total curvature of the simulated steady-state cutting front as an appropriate indicator for the cut flank roughness also in other parameter regimes.

Indication of the melt drag level

The laser beam cutting process is significantly determined by the laser beam parameters. Nevertheless, also the cutting gas parameters considerably influence the process and the related cut result. Therefore, CALCut also takes into account the gas parameters.

The most prominent effect of the cutting gas parameters in laser beam fusion cutting of stainless steel is the extent of dross attachment at the bottom edge and - in the worst case – the appearance of a melt drag due to a separation of the boundary layer of the supersonic flow from the cutting front. This can lead to significantly reduced driving forces on the melt film, being visible on the cut flanks as a level where pronounced melt drag starts to occur [14].

Even if the gas parameters are fixed, as it is the case in this study, their impact is strongly influenced by the laser beam parameters and the resulting kerf formation. The simulation reveals the corresponding interaction and calculates the maximum possible supersonic gas jet penetration at the selected cutting parameters (see section 2.1).

During the experiments, a quite high cutting gas pressure of 2 MPa was selected in order to avoid boundary layer separation in the kerf as far as possible. Nevertheless, at focal positions near to the surface of the workpiece the resulting narrow kerf entrance limits the gas jet coupling into the kerf so much so that a boundary layer separation causes a pronounced melt drag and deteriorates the cut flank appearance. Moreover, this effect typically comes along with clinging dross at the bottom cut edge.

Looking at **fig. 12**, at least a qualitative agreement of the calculated maximum jet penetration and the starting level of the melt drag on the cut flanks can be observed. Even if a nearly quantitative agreement might be concluded from **fig. 12**, the underlying physical approximation of the model is definitely too simple to meet such a claim in general.

Indication of the dross length

However, trends might be predicted by this indicator. Therefore, the simulated maximum jet penetration is compared with the maximum dross length versus focal position in **fig. 13**. And the result is quite convincing. Global and local trends of dross versus focal position are consistently described by a negative correlation with CALCut's maximum jet penetration with only 1 exception out of 12, i.e. one red line in the graph. The numbers in the black circles represent the focal position of each experimental point. The correlation coefficient of -0.83 definitely confirms a strong relationship of simulated indicator and practical quality feature.

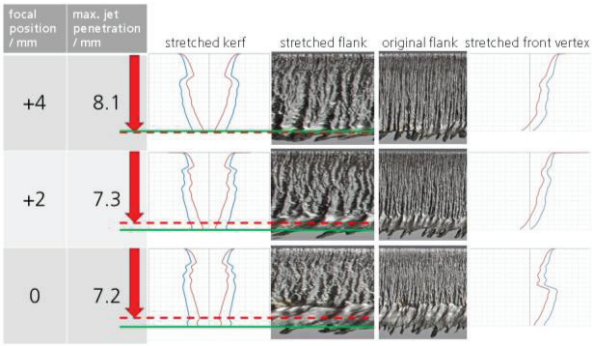

Fig. 12 Indication of an elevated melt drag level on the cut flank by a reduced maximum jet penetration indicator at focal positions too near to the surface.

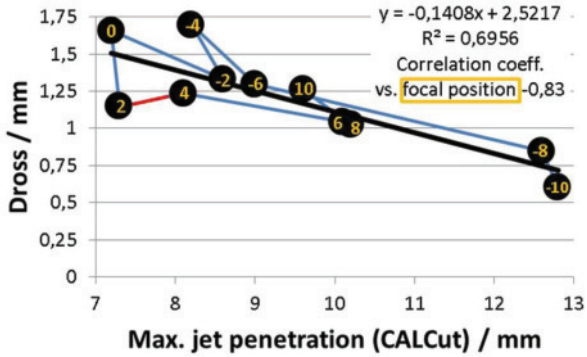

Fig. 13 Negative correlation of the maximum dross length and CALCut's maximum jet penetration indicator versus focal position. Global and local trends of dross vs. focal position are reliably described by CALCut's indicator with only 1 exception out of 12, i.e. one red line in the graph. The numbers in the black circles represent the focal position of each experimental point.

4. Conclusion

Fundamental questions have been answered with the help of the simulation tool CALCut:

Which melt film surface temperatures do occur? CALCut simulations reveal the dominant influence of the cutting speed on the temperature, reaching the vaporization threshold at about 5 m/min in 3 mm stainless steel and showing only slightly higher temperatures in case of 1 micron wavelength compared to 10 micron.

How do multiple reflections (MR) contribute to the process? MR is an essential feature of laser beam cutting at 1 µm and its consideration in CALCut is indispensable. The higher absorption at small angles of incidence leads to a wider kerf entrance while MR expands the central part of the kerf. Only MR enables an acceptable beam coupling in the kerf – about a factor of 2 higher than without MR contribution.

What are the essential mechanisms of kerf formation? The kerf formation is dominantly influenced by the laser beam parameters and results from the self-adjustment of the cutting front geometry according to the local power balance requirements. Simulated and practical kerf cross section are in good agreement.

Why do "black knots" and trisections arise in striation patterns? Such irregularities of the striation pattern on the cut flank are indicated by related irregularities at the simulated cutting front vertex and cutting flank. Black knots and trisection of the striation pattern can be understood as finger prints of related strong buckling at the quasi-steady-state cutting front.

It can be concluded that the simulation tool CALCut makes explainable and quantifiable:

- process efficiency,
- gas jet penetration depth,
- kerf width and cross-section profile,
- irregularities of the striation pattern such as
  - black knots
  - trisection
- quality features such as
  - cut flank roughness
  - dross attachment

The quality features could be correlated with CALCut indicators:

- The practically achievable cut flank roughness is found to correlate with the total curvature of the simulated 3-dimensional cutting front.
- The practical dross length shows a distinct, negative correlation with the calculated maximum penetration of the supersonic gas jet into the kerf.

Whenever questions arise regarding the efficiency, robustness and quality of cutting processes using new beam sources, new materials or new process regimes, CALCut provides the physical analysis to optimize the process above and beyond empirical values.

Acknowledgement

The research leading to these results has received funding from the European Union's Seventh Framework Programme within the Research for SMEs Project "FILCO - Fibre-delivered Laser Cutting Optimisation" under Grant Agreement number 315405 and within the ICT Collaborative Project "HALO - High power Adaptable Laser beams for materials prOcessing" under Grant Agreement number 314410. The funding is gratefully acknowledged. The author would also like to thank Norbert Wolf and Stoyan Stoyanov for the performance of the cutting experiments and Carmen Klein-Petring for the evaluation of the cut edges.

References

[1] Hirano, K, Fabbro, R: Experimental investigation of hydrodynamics of melt layer during laser cutting of steel, J. Phys. D: Appl. Phys. **44** (2011).

[2] Otto, A, Koch, H, Leitz, K H, Schmidt, M: Numerical Simulations - A Versatile Approach for Better Understanding Dynamics in Laser Material Processing, Physics Procedia **12**, 11-20 (2011).

[3] Petring, D, Molitor, T, Schneider, F, Wolf, N: Diagnostics, modeling and simulation: Three keys towards mastering the cutting process with fiber, disk and diode lasers, Physics Procedia **39**, 186–196 (2012).

[4] Petring, D: Application-oriented modeling of laser beam cutting for computer-assisted process optimization. PhD thesis RWTH Aachen University 1994, Shaker Verlag, Aachen, 1995 (in German)

[5] Petring, D: Computer simulation of laser cutting for the limiting-value-oriented development of robust processes, Welding and Cutting **4** No. 1, 37-42 (2005)

[6] Petring, D, Schneider, F, Wolf, N, Nazery Goneghany, V: How Beam Quality, Power and Wavelength Influence Laser Cutting and Welding Processes. Proc. of LAMP2009 - the 5th International Congress on Laser Advanced Materials Processing, Kobe, JP, June 2009

[7] Petring, D: Latest developments in the CO_2 versus fibre laser cutting debate. Industrial Laser Applications Symposium ILAS 2015, Kenilworth, Warwickshire, UK, March 2015

[8] Seefeld, T, and O'Neill, B: Cutting and welding with the new high brightness lasers. The Laser User, Issue 50, Spring 2008, 32-37

[9] Wandera, C, Kujanpää, V, Salminen, A: Laser power requirements for cutting of thick-section steel and effects of processing parameters on mild steel cut quality. Proceedings IMechE Part B, Journal of Engineering Manufacture, Volume 225, 2011

[10] Scintilla, L D, Tricarico, L, Mahrle, A, Wetzig, A, Beyer, E: Experimental investigation on the cut front geometry in the inert gas laser fusion cutting with disk and CO2 lasers. 30th International Congress on Applications of Lasers and Electro-Optics (ICALEO 2011), paper #105, Orlando, FL, USA, October 2011

[11] Olsen, F O: Laser cutting from CO_2 laser to disc or fiber laser – possibilities and challenges. 30th International Congress on Applications of Lasers and Electro-Optics

(ICALEO 2011), paper #101, Orlando, FL, USA, October 2011

[12] Scintilla, L D, Tricarico, L, Mahrle, A, Wetzig, A, Himmer, T, Beyer, E: A comparative study on fusion cutting with disk and CO2 lasers. 29th International Congress on Applications of Lasers and Electro-Optics (ICALEO 2010), paper #704, Anaheim, CA, USA, September 2010

[13] Hirano, K, Fabbro, R: Possible explanations for different surface quality in laser cutting with 1 and 10 µm beams. Journal of Laser Applications, Vol. 24, Number 1, February 2012

[14] Zefferer, H, Petring, D, Beyer, E: Investigations of the Gas Flow in Laser Beam Cutting. DVS-Berichte 135, Konferenz “Strahltechnik”, Karlsruhe, 210-214 (1991)